The DOI for this manuscript is doi: 10.1175/2009JPO4345.1

Numerical Investigation of Spectral Evolution of Wind Waves. Part 1. Wind Input Source Function

***K.N.Tsagareli*[1], *A.V.Babanin*[2]* , *D.J.Walker*[1], *I.R.Young*[3]**

[1] *School of Civil, Environmental and Mining Engineering, The University of Adelaide*

[2] *Faculty of Engineering and Industrial Science, Swinburne University of Technology*

[3] *Vice-Chancellor, Swinburne University of Technology*

* Corresponding author

Prof. Alexander Babanin

PO Box 218 Hawthorn

Victoria 3122 Australia

ababanin@swin.edu.au

Abstract

The current paper is dedicated to the investigation and calibration of the parameterised form for the wind-input source term S_{in} proposed earlier on the basis of field observations at Lake George, Australia. The main objective of this study was to obtain spectral forms for the wind input source function S_{in} which incorporates the novel observation-based features and at the same time satisfies the important physical constraint, that the total integrated wind input must agree with independently observed magnitudes of the wind stress. Within this approach, a new methodology – a dynamic self-adjusting routine was developed for correction of the wind-input source function S_{in}. This correction involves a frequency-dependent adjustment to the growth rate $\gamma(f)$, based on extrapolations from field data. The model results also show that light winds require higher-rate adjustments of the wind input compared to the strong winds.

1. Introduction

Wind wave prediction is undertaken by means of spectral numerical modelling of the physical processes responsible for wave development and wave evolution. The evolution of the wave spectrum is described by means of the radiative transfer equation, which in deep water can be written as:

$$\frac{\partial F}{\partial t} + c_g \times \nabla F = S_{tot} = S_{in} + S_{ds} + S_{nl} \qquad (1\text{-}1)$$

where $F = F(\mathbf{k}, \omega, \mathbf{x}, t)$ is the wave power spectrum, which depends on wavenumber $\boldsymbol{k}$, angular frequency ω, space $\mathbf{x}$ and time t, c_g is the group velocity of the waves, S_{tot} represents all energy fluxes contributing to wind-wave evolution. In deep water, it is generally accepted that wind-wave growth is a result of three physical processes: atmospheric input from the wind to the waves S_{in}, wave dissipation (due to breaking, interaction with turbulence and viscosity) S_{ds}, and nonlinear energy transfer between the wave components S_{nl}. All these source terms are spectral functions. Among them, the wind input term S_{in} is the focus of the present study.

Previously conducted observational and analytical studies developed various theories of wind-wave interaction (Jeffreys 1925; Miles 1957; Janssen 1991, among others) and different parameterised forms for the wind input source term S_{in} have been suggested. Some of these forms were developed on the basis of observational data (Snyder et al. 1981; Hsiao and Shemdin 1983; Donelan 1999), whereas other forms were developed as a result of modeling the air-sea boundary layer (Gent and Taylor 1976; Makin and Chalikov 1979; Al Zanaidi and Hui 1984; Chalikov and Makin 1991; Chalikov and Belevich 1993). However, no theory of wind wave interaction can be regarded as fully consistent and comprehensive (see Donelan et al. 2006; The WISE Group 2007 for discussions). The proposed theories need further development and thorough empirical verification. However, limitations of observational techniques and the complexity of the wind-wave interaction mechanisms create further difficulties both for the measurements and for such validations.

A range of parameterised forms are widely used in contemporary wave models, although most of them were only defined for some particular environmental conditions. Therefore, their general application is questionable. For example, the parameterisations presently employed in the third-generation wave models WAM (WAMDI Group 1988, Komen et al. 1994), SWAN (Booij et al. 1998), WAVEWATCH-III (Tolman and Chalikov 1996, Tolman 1997) were obtained for light to moderate winds and their use in strong wind conditions needs, at the very least, justification.

Furthermore, the recent observational findings at Lake George, Australia (AUSWEX experiment, Young et al. 2005; Donelan et al. 2005, 2006; Babanin et al. 2007) bring new insights to the physical processes of wind-wave interaction, particularly at strong and extreme wind-wave forcing conditions. These findings were implemented in a new parameterisation form of S_{in} (Donelan et al. 2006; Babanin et al. 2007) investigated in this paper.

This new parameterisation was able to reconcile apparently different observational outcomes for wind-wave growth rates obtained in well-developed oceanic conditions (Hsiao and Shemdin 1983) and strongly-forced and steep young waves (Donelan 1999). This was achieved by incorporating two newly observed features of wind-wave coupling, i.e. the dependence of the growth increment $\gamma(f)$ on wave steepness and full air-flow separation (and correspondingly, a relative reduction of the wind input) in extreme wind-forcing situations.

Before implementation in a spectral model as the wind-source term, the new parameterisation needed further research and adjustment. Whilst obtained over a relatively broad range of frequencies, its extrapolation into the higher-frequency spectral tail had to be investigated, as these are the scales which support most of the wind stress. Therefore, the overall objective of the present study was to develop an advanced parameterisation of the wind input source term, suitable for spectral modelling and satisfying the main physical constraint in the wave system. This constraint is the independently known wind stress, which has to agree with the total integrated wind input. In the course of the study, other physical properties of the wave field, i.e. shape of the high-frequency part of the wave spectrum, were also shown to be subject to the physical constraints imposed by the wind-wave coupling process.

In Section 2, necessary theoretical and experimental background to the topic is provided: parameterisation of the wind input, definitions for the total wind stress and drag coefficient. The approach, which is not only the tool, but is also one of the major results of this paper, is outlined in Section 3. Section 4 describes testing and calibration of the wind-input function employed, and Section 5 discusses outcomes and draws the conclusions. The present paper is accompanied by Part II (Babanin et al. 2009) which is dedicated to the constrained and observation-based dissipation function and evolution tests of the new wind input and dissipation.

2. **Background**

a. Growth Rate

Air-sea interaction results in a change in the properties of the wind-driven wavy surface, a change referred to as wave evolution. The energy and momentum fluxes across the air-water boundary layer determine the rate of wave evolution. Therefore, accurate modeling of these fluxes plays a significant role in wave prediction.

As the wind blows over young and moderately-developed waves, wave energy increases in time and space. Miles (1957) defined the temporal growth rate γ to describe the wave energy increase as

$$\gamma = \left(\frac{1}{\omega F}\right)\frac{\partial F}{\partial t}. \qquad (2\text{-}1)$$

Such a growth rate can be directly measured in wave experiments, both in the laboratory and in the field (e.g. Donelan 1999, Donelan et al. 2005).

It is well known that most of the momentum flux from wind to waves is supported by the component of pressure correlated with the wave slope (see Young 1999; Donelan 1999; Donelan et al. 2005, 2006):

$$\frac{\partial F(\omega)}{\partial t} = S_{in}(\omega) = \frac{1}{\rho_w g}\overline{p(x,t)\frac{\partial \eta_w(x,t)}{\partial t}} \qquad (2\text{-}2)$$

where $S_{in}(\omega)$ is the one-dimensional wind-input source function, $p(x,t)$ is the pressure exerted by the wind on the water surface, $\eta_w(x,t) = a\cos(kx-\omega t)$ is the surface elevation of amplitude a, and the overbar indicates averaging in time.

Most wind-input measurement data are presented as simultaneous records of pressure and surface elevation. These records can be converted into Fourier space giving the quadrature spectrum, $Q(\omega) = \frac{1}{\omega}\overline{p\frac{\partial \eta_w}{\partial t}}$. The quadrature spectrum can be further used to determine the non-dimensional growth rate $\gamma(\omega) = \frac{Q(\omega)}{\rho_a g F(\omega)}$ (see Donelan et al. 2006). Thus, the wind input source term can be estimated as:

$$S_{in}(f) = 2\pi \rho_a/\rho_w\, f\gamma(f)F(f) \qquad (2\text{-}3)$$

where ρ_a is density of the air and ρ_w is density of the water and $f=\omega/2\pi$ is the frequency.

Existing observational data for the growth rate, however, are contradictory and obscure. The Australian Shallow Water Experiment (AUSWEX) was undertaken at

Lake George, Australia in 1997-2000 in order to study wind-wave coupling and wave breaking processes with the purpose of parameterising the respective source functions. A comprehensive description of the experiment and relevant techniques developed during this study has been given in Young et al. (2005) and, with respect to measurements of the wind input in Donelan et al. (2005). This study was distinctly different from previous field studies because it was the first attempt to measure the pressure growth term for strongly-forced and steep waves. In Lake George, the depth-limiting conditions made it possible to study a wide range of wind forcing circumstances including very young waves, with U_{10}/c_p = 5.1–7.6 and U_{10}/c ranging up to 11.2, with varying wave steepness (here, U_{10} is the wind speed at standard 10m height and $c(f)$ is the phase speed of waves with frequency f, i.e. c_p is the phase speed of waves at the spectral peak f_p). This study revealed previously unrecognised features of wind-wave interaction, namely: 1) wind-flow separation from the water surface during very strong winds reduces wind energy transfer to the waves; 2) the wave growth rates γ depend on wave steepness; 3) wind-input fluxes double over breaking waves. Furthermore, this study proposed a new parameterised form for the wind input source term S_{in} which accounted for these new features (Donelan et al. 2006, Babanin et al. 2007).

Previously, based on potential theory for gravity waves, the growth rate γ was considered a parameter unrelated to wave steepness. The Lake George experiment showed, however, that both the phase shift and the normalised induced pressure amplitude are connected to the wave steepness and approach their potential flow values only when $ak \rightarrow 0$. The experiment at Lake George resulted in a wave growth rate relationship of the form:

$$\gamma = G\sqrt{B_n} \cdot \left[\frac{U_{10}}{c} - 1\right]^2 \qquad (2\text{-}4)$$

where γ is the growth rate, $B_n(\omega) = \frac{\omega^5 F(\omega)}{2g^2} A(\omega)$ is the normalised spectral saturation (Donelan et al. 2006) used as a spectral analogue of wave steepness, A is the directional spreading function according to Babanin and Soloviev (1987, 1998a) and G is the sheltering coefficient which accounts for the effect of full flow separation on wave growth:

$$G = 2.8 - 1.0 \cdot (1 + \tanh(10 \cdot \sqrt{B_n} \cdot \left[\frac{U_{10}}{c} - 1\right]^2 - 11)) . \qquad (2\text{-}5)$$

The function (2-5) is an analogue of the Heaviside step function used for a smoothed representation of the flow-separation effect. Thus, the results of the Lake George experiment showed that previously suggested wind-wave coupling theories and their respective parameterisations needed thorough revision due to inconsistencies and previously overlooked physics of air-sea interaction.

b. Wind Stress

The generation of waves on the water surface by the action of wind is due to work done by the wind stress exerted on this surface. Wind stress is a result of the air-sea interaction, i.e. ‘friction’ of air flow against the water surface, and reflects the strength of this interaction. Physically, it is the drag force per unit area exerted on the water surface by the adjacent layer of the airflow. Therefore, wind stress determines the exchange of momentum between the atmosphere and the water surface.

Significant stresses arise within the near-surface atmospheric boundary layer because of the strong shear of the wind between the slowly moving air near the water surface and the more rapidly moving air in the layer above (see e.g. Komen at al. 1994). Close to the surface, the total wind stress τ can be represented by three components: 1) the turbulent stress τ_t, 2) the wave-induced stress τ_w, and 3) the viscous or tangential stress τ_v:

$$\tau = \tau_t + \tau_w + \tau_v \tag{2-6}$$

(e.g. Kudryavtsev et al. 2001). The atmospheric turbulent momentum flux decreases to zero at the surface where the turbulence vanishes. Therefore, at the surface the total wind stress is a combination of the wave-induced stress τ_w induced by the ocean waves and the viscous stress τ_v generating the surface currents directly.

c. *Drag Coefficient*

Wind stress depends on the roughness of the underlying surface. Over the ocean, this roughness changes as the waves develop. In light winds, the sea surface is calm and aerodynamically smooth. Wind stresses exerted on the sea surface are, therefore, small. In strong winds, particularly when the waves are actively breaking, the surface is aerodynamically rough and the wind stresses are large. Thus, the wind-wave coupling determines the drag force over the sea surface.

The drag coefficient is used to translate wind measurements in the boundary layer to the wind stress at the surface:

$$\tau = \rho_a C_D U_{10}^2 = \rho_a u_*^2 \tag{2-7}$$

where, C_D is the drag coefficient, and u_* is the so-called friction velocity, i.e. a dimensional measure of the surface stress.

According to (2-7), the total wind stress can be estimated if the wind speed U_{10} is measured and the drag coefficient C_D is known. The drag coefficient depends on the wave field and on the turbulent structure of the flow in the air and the water in a very complicated manner. It has been generally accepted that the drag coefficient increases with the wind speed, but the scatter of such dependences has always been very large.

At strong winds, recent observations show that the drag coefficient approaches some limiting value (e.g. Powel et al. 2001, Donelan et al. 2004, Makin 2005), but overall it depends on a large number of air and sea properties (for example, 15 such characteristics are listed in Babanin and Makin 2008).

3. The Approach

a. Computational aspects

In the present study, computations of the wind input source term, as given by Donelan et al. (2006), were initially performed for different wind speeds U_{10} = {7m/s, 10m/s, 15m/s and 20m/s} and for different stages of wave development U_{10} / c_p = {5.8, 2.7 and 0.82}. Due to the similarity of the results, only cases for the wind speed U_{10} = 10 m/s are shown. In addition, computations were performed for two different types of wave spectra, JONSWAP (Hasselmann et al. 1973) and DHH (Donelan et al. 1985). In Part II (Babanin et al. 2009), a spectral shape parameterisation which contains both f^{-4} and f^{-5} subintervals of the spectral tail is suggested.

Parameters of the wave spectra at different stages of wave development were determined as functions of the wind forcing parameter, U_{10}/c_p. Relationships from the Black Sea experiments reported by Babanin and Soloviev (1998b) were used for the shape parameters of the JONSWAP spectra. For the DHH spectra, relationships from the measurements taken at Lake Ontario (Donelan et al. 1985) were used. All computations were performed using the full band of wave scales within the gravity-wave range. Therefore, a discrete frequency spectral grid was defined between the lower and upper limits of f_{min} = 0.05Hz and f_{cut} = 10Hz, respectively.

b. Wave-Induced Stress

In the present study, momentum flux across the water surface was considered as the key boundary parameter for calibrating the wind-input source function. Among the different contributions to the total stress (2-6), the wave-induced stress is directly related to the energy exchange between the wind and the waves and is used as an important constraint for the wind-input source term. It is estimated at the air-sea interface as:

$$\tau_w = \tau - \tau_v . \tag{3-1}$$

On the other hand, the wave-induced stress is determined by the wind momentum input function as:

$$\tau_w' = \int_{f_{\min}}^{f_{cut}} M(f) df \tag{3-2}$$

where *M(f)* is the wind momentum-input source function. The momentum-input function *M(f)* can be obtained from the wind energy-input source term $S_{in}(f)$:

$$M(f) = \rho_w g \frac{S_{in}(f)}{c(f)} \tag{3-3}$$

where g is gravitational acceleration. Therefore:

$$\tau_w' = \rho_w g \int_{f_{\min}}^{f_{cut}} \frac{S_{in}(f)}{c(f)} df . \tag{3-4}$$

The principal constraint, imposed in this paper on the wind-input function S_{in}, being calibrated, is that the integrated wave-induced stress τ'_w (3-4) should be equal to τ_w (3-1):

$$\tau_w' = \tau_w . \tag{3-5}$$

This constraint is clearly apparent from the physical point of view, but is hardly ever employed because routinely the computational range of spectral wave models is limited by a relatively low-frequency upper cut-off in the vicinity of the spectral peak. In this regard, credit has to be given to Mark Donelan who suggested the (3.5)-like condition as a general criterion for testing wave spectral models at the WISE-2004 meeting in Reading, UK. In this study, satisfying this criterion determines the credibility of a parameterised form for the wind input source term S_{in}, and also sets the main physical framework for investigation of the behaviour of this parameterisation and its validation.

Wave-induced stress is dependent on the upper limit of the integral in (3-4). The contribution of the short-wave scales to the total stress is significant, and therefore the higher the upper limit of the integral, the more precise the estimate of the wave-induced stress. Therefore, the upper limit of f_{max} = 10Hz was selected for the integral (3-4) signifying the shortest waves in the capillary range still involved in air-sea coupling.

Computation of the wave-induced stress using (3-1) required knowledge of the viscous stress. Here, the viscous stress contribution to the total stress was estimated according to Banner and Peirson (1998). Substituting their $\tau_v = \rho_a C_V U_{10}^2$, where C_V is the viscous drag coefficient, along with (2-7) into (3-1) yields:

$$\tau_w = \rho_a U_{10}^2 (C_D - C_V)\,. \tag{3-6}$$

Banner and Peirson (1998) demonstrated a qualitative trend of the viscous stress as a function of the wind speed, but did not present a quantitative dependence. In the present study, the data of Banner and Peirson (1998) were digitised and parameterised as a function of wind speed U_{10}:

$$C_V = -5 \cdot 10^{-5} U_{10} + 1.1 \cdot 10^{-3}\,. \tag{3-7}$$

We also considered the discrepancies between the drag coefficients C_D previously proposed by different researchers. A great number of experimental studies have resulted in a situation where various researchers are divided in their opinions and have produced a variety of parameterisations for the sea drag (see e.g. Babanin and Makin 2008 for a review). Most common are dependences for the drag coefficient C_D as a function of wind speed U_{10} or the wind-forcing parameter U_{10}/c_p. Both types of C_D dependences were employed in the present paper, i.e. the parameterisation of Garratt (1977) in terms of wind speed and the expressions suggested by Guan and Xie (2004), based on a review of earlier parameterisations, in terms of wave age.

We should point out that the chosen parameterisations may differ quantitatively from others available, but this difference is not a major issue as far as the outcomes of the present study are concerned. Because of the scatter of the sea-drag dependences, errors due to normalisation based on the total stress employed here may be of the order of tens of percent, whereas errors due to the absence of such a normalisation are of the order of hundreds of percent, as argued below.

According to Garratt (1977), the drag coefficient is

$$C_D \cdot 10^{-3} = 0.067 U_{10} + 0.75 . \qquad (3.8)$$

The wave-age dependent drag coefficient $C_D(U_{10}/c_p)$ was computed on the basis of the review by Guan and Xie (2004):

$$C_D = [0.78 + 0.475 \cdot f(\delta) \cdot U_{10}] \times 10^{-3} \qquad (3\text{-}9)$$

where

$$f(\delta) = 0.85^B A_G^{\ 1/2} \delta^{-B} \qquad (3\text{-}10)$$

and the wave age dependence is included through the wave steepness $\delta = H_s \omega_p^2 / g$. Here, H_s is the significant wave height, ω_p is the radian peak frequency, and the empirical parameters A_G = 1.7 and B = -1.7 are chosen such that C_D in (3-9) is in agreement with results of Drennan et al. (2003).

The resulting computations of wave-induced stress τ'_w using (3-4) and τ_w using (3-6) are compared in Figures 1 and 2. Since the integral in (3-4) depends on the wave spectrum used to obtain the wind input $S_{in}(f)$ in (2-3), the computations were performed both for JONSWAP and DHH spectra at different stages of wave development, in Figure 1 and Figure 2 respectively.

Figure 1 shows the JONSWAP-based results of computations of the integrated wave-induced stress τ'_w, using parameterised forms for $\gamma(f)$ in the wind-input source term S_{in} according to Donelan et al. (2006), Donelan (1999), Hsiao and Shemdin (1983) and Snyder et al (1981). All parameterisations, except those of Snyder (1981) and Donelan et al. (2006) for young waves, give noticeably larger values of wave-induced stress compared to those from the stress-balance equation (3-6). This means that all these parameterised forms, as they were originally proposed, require further calibration, particularly for mature wave ages. The wave-induced stress increases with wave development until the inverse wave age reaches U_{10} / c_p = 1.5, whereupon a decreasing trend is clearly seen. This behaviour is the result of applying the wave-age dependence obtained by Babanin and Soloviev (1998b) for the JONSWAP spectral shape parameters, principally the spectrum-tail level α. At the U_{10} / c_p = 1.5 maximum, the magnitudes of the τ'_w stress, computed for the Donelan et al. (2006) wind input, is more than two times greater than the value of wave-induced stress expected from the τ_w dependences.

Figure 2, based on the DHH spectral form, estimates S_{in} by means of (2-3) and shows significantly larger differences between stresses τ'_w and τ_w. The ratio is now of the order of 30-50 rather than the order of 2. Furthermore, the stresses τ'_w computed for S_{in} by means of the Donelan et al. (2006) parameterisation have the largest values, indicating the greatest disagreement with the criterion (3-5). Most of this striking and dramatic difference is apparently due to differences in the parameterisations of the spectral tail; that is f^{-5} in JONSWAP and f^{-4} in DHH. While the latter is a definite experimental observation, also justified theoretically (e.g. Zakharov and Zaslavskii 1983), a transition from the f^{-4} slope to f^{-5} has to occur at some smaller scales in the spectral tail in order for the integral (3-4) to converge to realistic values of the total stress. Such a transition is also supported experimentally (e.g. Forristal 1981, Kahma and Calkoen 1992, Babanin and Soloviev 1998a, Resio et al. 2004).

4. Calibrating the New Wind-Input Function

The calibration was conducted by tests with a constant-speed wind. The wave spectrum changes as waves develop, and so does the wind input (2-3) and wave-induced stress (3-2). However, the integral of the wind-input source function S_{in} must be consistent with the criterion (3-5), regardless of the wave-spectrum shape or wave-development stage. Therefore, in the model testing, consistency of the condition (3-5) had to be verified at every step in order to determine whether the wind-input source term needs to be corrected.

Correction of the wind input spectrum can be performed by applying a correction coefficient to the wind-input source function, thus increasing or decreasing the integral value in (3-4). To achieve this, the ratio of wave-induced stresses τ_w / τ'_w can be used as the correction coefficient, dependent on wave-development conditions. Initially it was assumed that the correction coefficient τ_w/τ'_w should be applied to the wind-input source function over the entire frequency range.

The majority of previous experimental wind-input estimates were performed for the range of frequencies close to the peak frequency [$0.7f_p$, $1.3f_p$]. In Donelan et al.

(2006), some measurements were conducted up to $2f_p$ and even up to $4f_p$, but this is still only a relatively small fraction of the spectral tail which supports a major part of the wind stress. Therefore, the high-frequency range can be considered an acceptable domain for adjustments to the parameterisation necessary to satisfy the constraint (3-5). In the present study, the wind-input source function S_{in} suggested by Donelan et al. (2006) is investigated and adjusted in this high-frequency range.

Accordingly, the correction coefficient should be determined in the range of frequencies starting from $f_0 > f_p$, which is the lower boundary of the operational frequency domain in which the correction can be applied. Because of this, the correction coefficient will be also dependent on the choice of f_0 rather than simply the stress ratio τ_w/τ'_w. The correction coefficient defined in this way is denoted as X. It is desirable that a choice of f_0 does not extend into the dominant wave scales where the experimental data of Donelan et al. (2006) were obtained and therefore the correction should not be applied. Therefore, the lower frequency f_0 for the operational frequency domain was chosen as $f_0 = 1.35 f_p$.

In the experiments, the separation effect (as well as the other parameterised effects) was only observed at frequencies below f_0. For some spectra, the separation zone is located at higher frequencies – in such cases the correction is applicable to the separation effect also. When the separation occurs at $f<f_0$, no correction to the separation parameterisation is applied.

In order to determine the correction factor X, the integration in (3-2) was split into two ranges of $[f_{min}, f_0]$ and $[f_0, f_{cut}]$:

$$\tau'_w = \int_{f_{\min}}^{f_0} M(f)df + \int_{f_0}^{f_{cut}} M(f)df \, . \qquad (4\text{-}1)$$

For convenience we denote these two integrals as

$$S_1 = \int_{f_{min}}^{f_0} M(f)df \text{ and } S_2 = \int_{f_0}^{f_{cut}} M(f)df \tag{4-2}$$

with the correction factor X to be applied to the second integral S_2. Taking into account (3-5), (4-1) and (4-2), we have:

$$\begin{cases} \tau_w = S_1 + X \cdot S_2, \\ \tau_w^{'} = S_1 + S_2, \end{cases} \tag{4-3}$$

that is

$$X = 1 + \frac{\tau_w - \tau_w^{'}}{S_2} \quad . \tag{4-4}$$

The difference between the stresses τ_w and τ'_w in (4-4) determines whether an increase ($X > 1$) or reduction ($X < 1$) of S_{in} is required. Negative X, which would signify energy flux from the waves to the wind, was not allowed here, and therefore this additional constraint was imposed:

$$1 + \frac{\tau_w - \tau_w^{'}}{S_2} > 0 \, . \tag{4-5}$$

Condition (4-5) can be rewritten as

$$S_2 > \tau_w^{'} - \tau_w \, , \tag{4-6}$$

and since $S_2 = \tau_w^{'} - S_1$, it follows:

$$S_1 < \tau_w \, . \tag{4-7}$$

In most cases of wave development, condition (4-7) is true. In order to have this condition true for all cases, the correction X was required to readjust the operational frequency domain if necessary. Integral S_1 depends on the choice of the starting frequency f_0, and thus the limitation (4-7) was translated into a limiting condition for the starting frequency f_0. In the case of $X < 0$, the starting frequency f_0, instead of

$1.35f_p$, was made the frequency closest to $1.35\,f_p$, for which the condition (4-7) is still true.

Figure 3 shows a comparison of the wind input source terms computed for the JONSWAP and DHH spectra before and after correction by means of the factor X. The wind-input source functions after correction have a distinct discontinuity at the frequency f_0. This discontinuity in the magnitude of the wind-input spectrum is greater for the DHH wave spectrum compared to the JONSWAP spectrum, because of the required rate of reduction for the total stress. In nature, however, such sudden changes of behaviour across the continuous spectrum can hardly be expected. Therefore, it was necessary to smooth the transition at the frequency f_0.

It should be stressed that the relatively steep jump in all the spectra around 0.8Hz is not an artefact of the smoothing procedure, but is the consequence of the Donelan et al. (2006) parameterisation. As mentioned above, this parameterisation predicts full flow separation at some wind-forcing/wave-steepness conditions, and a corresponding reduction of the wind input. The 0.8Hz jump reflects the transition from the non-separated to the fully separated flow according to Donelan et al. (2006).

In order to remove the discontinuity, the correction factor X could not remain a simple function of the wind forcing U_{10}/c_p only, and at each stage of wave development it was made a frequency-dependent function $X(f)$. In the present study, this function was termed $L(f)$, the correction function, to differentiate it from the correction factor $X(U_{10}/c_p)$.

Selection of the correction function was based on satisfying a set of specific requirements:

- The correction function $L(f)$ must be a monotonic continuous function;
- $L(f)$ must have a smooth transition at the frequency f_0: $L(f_0) = 1$;

- The wave-induced stress τ'_w, computed for $L(f)S_{in}(f)$ must be consistent with τ_w;
- The magnitudes of $L(f)S_{in}(f)$ for very small-scale waves must be comparable to the spectral magnitudes of the wave spectral dissipation function S_{ds}. Otherwise, the dissipation will prevail at high-frequency spectral components, which can cause singularities during wave development.

Based on these requirements, the following function was selected:

$$L(f) = \exp\left(\frac{f_0 - f}{f} \cdot \eta\right) \tag{4-8}$$

where η is a correction rate which is computed from the stress condition (4-4), i.e.

$$\eta = \frac{f_i \ln X}{f_0 - f_i} \tag{4-9}$$

and f_i is the frequency between f_0 and f_{cut} such that $L(f_i) = X$. The parameter η determines the slope of the wind-input source function tail in the range of frequencies $f > f_0$ and depends on the wind-forcing condition U_{10} / c_p. Results of the smoothing by means of the $L(f)$ function are illustrated in Figure 4 for the JONSWAP-based S_{in}.

The correction of the wind-input function, therefore, relies on the determination of the $L(f)$ function when the condition $\int_{f_0}^{f_{cut}} L(f)M(f)df = X \int_{f_0}^{f_{cut}} M(f)df$ is true. This correction method, was performed as a dynamic self-adjusting routine in further numerical wave modelling of (2-1). The routine was termed dynamic as the correction routine is applied to the computation of the wind-input source term at every stage of wave development. The dynamic self-adjustment routine includes computations of the wave-induced stress at each stage of wave development and the outcome is a corrected wind-input source term.

5. Results and Discussion

The correction was applied to the wind-input source function suggested by Donelan et al. (2006) and computed for the JONSWAP and DHH spectra at different stages of wave development. Furthermore, the spectra of the resulted growth rate $\gamma(f)$, computed for the JONSWAP and DHH spectra, were analysed.

Figure 5 shows a comparison of the wind-input source term S_{in} before and after the correction applied by means of the function $L(f)$ (4-8). Whilst initial values of S_{in} for the tail regions of the JONSWAP and DHH spectra differ very significantly, this difference is greatly reduced by the correction procedure. This demonstrates the effectiveness of the routine in producing reasonably consistent magnitudes of the wind-input across the spectrum, regardless of the input wave spectra. The spectral form does, however, impact on the distribution of $S_{in}(f)$ with frequency, particularly in the high-frequency domain.

In Figure 6, the growth rate functions $\gamma(f)$ are plotted before and after the stress correction, computed for the JONSWAP wave spectrum of moderately young waves with $U_{10} / c_p = 2.7$. As shown in this figure, the corrections lead to a reduced source term slope, as a function of frequency. A similar trend is observed in Figure 7 for growth rates computed for the DHH spectrum. In this case, the change of frequency dependence is greater, but the corrected $\gamma(f)$ behaviour comes close to that based on the JONSWAP spectrum. These points again demonstrate the consistency of the corrections made on the basis of the physical constraints for quite different input conditions.

Figure 8 illustrates results of the correction of the wind-input source functions at different stages of wave development, for the wind speed U_{10} = 10 m/s, based on the JONSWAP spectra. The high frequency tails of the wind-input source term have similar slopes, except for the case of full development where the slope is slightly reduced. The magnitudes of the wind input source terms are determined by the magnitudes of the energy density spectrum (JONSWAP spectrum in this case), and differ significantly. In this study, the Babanin and Soloviev (1998b) parameterisations for the spectral-shape parameters of the JONSWAP spectrum were used to compute the JONSWAP spectra at different stages of wave development. The transition from fully-separated flow to non-separated flow is confined to the relatively narrow range of frequencies near f_t = 1Hz.

Figure 9 shows the corrected wind-input source term distributions based on the DHH wave spectra at the same stages of wave development as above. Interestingly, in this case, i.e. the case of an f^{-4} wave-spectrum tail, the slopes of the wind-input $S_{in}(f)$ high frequency tails are different at each stage of wave development. However, unlike the JONSWAP case, at high frequencies (f > 3Hz) the input source function tails are all close to each other except for very young waves.

Finally, the correction rates η as a function of wind forcing are plotted in Figures 10 and 11. The function $\eta(U_{10} /c_p)$ shows the rate of suppression of the wind-input source function which is the result of the stress correction at different stages of wave development (see 4-8,4-9). Figure 10 was obtained for JONSWAP spectra at different stages of wave development. As can be seen, the behaviour of this function depends on the type of drag-coefficient dependence chosen for computation of the wave-induced stress in (3-6). For waves with U_{10} /c_p > 1.6, the suppression is higher when using $C_D(U_{10})$. For the drag-coefficient $C_D(U_{10}/c_p)$ parameterisation, the maximum suppression of the wind-input function occurred at U_{10}/c_p = 1.6 (well-developed waves), while for $C_D(U_{10})$ it was at U_{10} / c_p = 4.1 (very young waves). For both types of the drag dependences, there is a step at U_{10} / c_p = 4.5, which corresponds to the transition of wind flow over dominant waves from fully-separated to non-separated.

The correction rates η obtained for DHH spectra as a function of wave development appear quite different in Figure 11. This figure, however, also shows the significant influence of the type of drag-coefficient dependence employed. Furthermore, the values of η (i.e. the required suppression) are much greater compared to the case of the JONSWAP spectrum. As already discussed, this is due to the f^{-4} tail in DHH, as opposed to f^{-5} in JONSWAP. The higher levels of the spectral tail produce greater contributions to the total wind input and require larger corrections to bring them down to realistic integral values of the total stress (see also Figures 1 and 2). For $C_D(U_{10}/c_p)$-dependence, the correction rate remains almost constant in the course of wave development, and even the step associated with the wind flow changing from fully-separated to non-separated flow is relatively mild.

The main conclusions of the study can be summarised as:

1. The physical framework for testing the frequency distribution of the wind input source term $S_{in}(f)$ in the present study was built on one of the important physical characteristics of wind-wave interaction – wave-induced stress τ_w – which can be directly and independently measured. The wave-induced stress τ'_w computed via integration of $S_{in}(f)$ should not exceed τ_w. This *stress consistency criterion* was used as the main constraint for verifying the consistency of wind-input parameterisation forms, and for subsequent calibration.

2. Previously suggested parametric forms (Snyder et al. 1981; Hsiao and Shemdin 1983; Donelan 1990; Donelan et al. 2006) were tested using the stress consistency criterion. The results show remarkable disagreement both between the forms and also with the total-stress measurements. The form of the spectral tail of the wave spectrum(f^{-4} or f^{-5}) also greatly impacts the results. In the case of an f^{-4} tail, the integrated wind input can exceed the total stress based on known parameterisations of the sea drag by a factor of 50 or more.

3. A dynamic self-adjustment routine, where the wave-induced stress is employed as the main physical constraint determining the momentum transfer from the wind to waves, was developed. The correction is applied in the region above the spectral peak, where measurement outcomes are presently not certain. The dynamic self-

correction routine is applicable to any parametric form of the wind-input source term employed in operational wave modelling (at the expense of some increase of the computational time). In the present study, its impacts were investigated by means of the Donelan et al. (2006) parameterisation.

4. The wind-input source function was examined in terms of the correction rate η. Results show that light winds require higher suppression rates than strong winds. Furthermore, the results indicate that the correction rates are highest in the range of wind forcing U_{10} / c_p =2 to 4, where transition of the wind flow over the dominant waves (spectral peak) from the fully-separated to the non-separated flow occurs.

Acknowledgments. We are very grateful for the suggestions provided by Erick Rogers from the Naval Research Laboratory.

References

Al-Zanaidi, M.A., and W.H. Hui, 1984: Turbulent air flow over water waves – a numerical study. *J. Fluid Mech.*, 148, 225 – 246

Babanin, A.V., and Yu.P. Soloviev, 1987: Parameterization of width of directional energy distributions of wind-generated waves at limited fetches. *Izvestiya, Atmospheric and Oceanic Physics*, 23, 645-651

Babanin A.V., and Y.P. Soloviev Y.P., 1998a: Variability of directional spectra of wind-generated waves, studied by means of wave staff arrays. *Marine Freshwater Res.*, 49, 89 – 101

Babanin A.V., and Y.P. Soloviev, 1998b: Field investigation of transformation of the wind wave frequency spectrum with fetch and the stage of development. *J. Phys. Oceanogr.*, 28, 563 – 576

Babanin, A.V., M.L. Banner, I.R. Young, and M.A. Donelan, 2007: Wave follower measurements of the wind input spectral function. Part 3. Parameterisation of the wind input enhancement due to wave breaking. *J. Phys. Oceanogr.*, 37, 2764–2775

Babanin, A.V., and V.K. Makin, 2008: Effects of wind trend and gustiness on the sea drag: Lake George study. *J. Geophys. Res.,* 113, C02015, doi:10.1029/2007JC004233, 18p

Babanin, A.V., K.N. Tsagareli, I.R Young, and D.J. Walker, 2009 : Numerical investigation of spectral evolution of wind waves. Part 2. Dissipation function and evolution tests. *J. Phys. Oceanogr.*, submitted

Banner, M.L. and W.L. Peirson, 1998: Tangential stress beneath wind-driven air-water interfaces. *J. Fluid Mech.,* 364, 115-145

Booij, N., L.H. Holthuijsen, and R.C. Ris, 1996: The SWAN wave model for shallow water. *Int. Conf. in Coastal Eng.*, ASCE, Orlando, 668 – 676

Chalikov, D.. and V.K. Makin, 1991: Models of the wave boundary layer, *Boundary Layer Meteorol.*, 56, 83 – 89

Chalikov, D., and M.Y. Belevich, 1993: One-dimensional theory of the wave boundary layer. *Boundary Layer Meteorol.*, 63, 65 – 96

Donelan M.A., J. Hamilton, and W.H. Hui, 1985: Directional spectra of wind-generated waves, *Philos. Trans. R. Soc. Lond.*, A315, 509-562

Donelan M.A., 1999: Wave-induced growth and attenuation of laboratory waves. In *Wind-over-Wave Coupling*. *Perspective and Prospects*, S.G. Sajadi, N.H. Thomas and J.C.R. Hunt, Eds., Clarendon Press, Oxford, 183 – 194

Donelan, M.A., B.K. Haus, N. Reul, W.J. Plant, M. Stiassne, H.C. Graber, O.B. Brown, E.S. Saltzman, 2004: On the limiting aerodynamic roughness in very strong wind. *Geophys. Res. Lett.*, 31, L18306, doi:10.1029/2004GL019460

Donelan, M.A., A.V. Babanin, I.R. Young, M.L. Banner, and C. McCormick, 2005: Wave follower field measurements of the wind input spectral function. Part I. Measurements and calibrations, *J. Atmos. Oceanic Tech.,* 22, 799–813

Donelan, M.A., A.V. Babanin, I.R. Young, M.L. Banner, 2006: Wave follower field measurements of the wind input spectral function. Part II. Parameterization of the wind input. *J. Phys. Oceanogr.*, 36, 1672-1688

Drennan, W.M., H.C. Graber, D. Hauser, and C. Quentin, 2003: On the wave age dependence of wind stress over pure wind seas. *J. Geophys. Res.*, 108, doi:10.1029/2000JC000715

Forristall, G.Z., 1981: Measurements of a saturation range in ocean wave spectra. *J. Geophys. Res.*, 86, 8075 – 8084

Garratt, J.R.D., 1977: Review of drag coefficients over oceans and continents. *Mon. Wea. Rev.*, 105, 915-929

Gent P.R., and P.A. Taylor, 1976: A numerical model of air-flow above water waves, *J. Fluid Mech.*, 77, 105 – 128

Guan, C.L., and L. Xie, 2004: On the linear parameterisation of drag coefficient over sea surface. *J. Phys. Oceanogr.*, 32, 2847–2851

Hasselmann, K., T.P. Barnett, E. Bouws, H. Carlson, D.E. Cartwright, K. Enke, J.A. Ewing, H. Gienapp, D.E. Hasselmann, P. Kruseman, A. Meerburg, P. Muller, D.J. Olbers, K. Richter, W. Sell, and H. Walden, 1973: Measurements of wind-wave growth and swell decay during the Joint North Sea Wave Project (JONSWAP). *Dtsch. Hydrogh. Z. Suppl.*, A8, 1-95

Hsiao S.V., and O.H. Shemdin O.H., 1983: Measurements of wind velocity and pressure with wave follower during MARSEN. *J. Geophys. Res.*, 88, 9841 – 9849

Janssen, P.A.E.M., 1991: Quasi-linear theory of wind-wave generation applied to wave forecasting. *J. Phys. Oceanogr.*, 21, 1631 – 1642

Jeffreys, H., 1925: On the formation of waves by wind. II. *Proc. Roy. Soc.*, A110, 341–347

Kahma, K.K., and C.J. Calkoen, 1992: Reconciling discrepancies in the observed growth of wind-generated waves. *J. Phys. Oceanogr.*, 22, 1389 – 1405

Komen, G.J., L. Cavaleri, M. Donelan, K. Hasselmann, S. Hasselmann, and P.A.E.M. Janssen , 1994: *Dynamics and modelling of ocean waves*. Cambridge Univ. Press, 532p

Kudryavtsev, V.N., V.K Makin, and J.F. Meirink, 2001: Simplified model of the air flow above the waves. *Boundary Layer Meteorol.*, 98, 155-171

Makin, V.K., and D.V. Chalikov, 1979: Numerical modelling of air structure above waves, *Izvestiya, Atmospheric and Oceanic Physics*, 15, 199 – 204

Makin, V.K., 2005: A note on drag of the sea surface at hurricane winds. *Boundary Layer Meteorol.*, 115, 169-176

Miles, J.W., 1957: On the generation of surface waves by shear flows. *J. Fluid Mech.*, 3, 185 – 204

Powel, M.D., R.J. Vickery, and T.A. Reinhold, 2003: Reduced drag coefficient for high wind speeds in tropical cyclones. *Nature*, 422, 279-283

Resio, D. T., C. E. Long, and C. L. Vincent 2004: Equilibrium-range constant in wind-generated wave spectra. *J. Geophys. Res.*, 109, C01018, doi:10.1029/2003JC001788.

Snyder, R.L., F.W. Dobson, J.A. Elliot, and R.B. Long, 1981: A field study of wind generation of ocean waves. *J. Fluid Mech.*, 102, 1– 59

Tolman, H.L., and D. Chalikov D., 1996: Source terms in a third-generation wind wave model. *J. Phys. Oceanogr.*, 26, 2497 – 2518

Tolman, H.L., 1999: User manual and system documentation of WAVEWATCH-III, version 1.18, *NCEP/NOAA Tech. Note*, 116, 110p

The WAMDI Group (Hasselmann, S., K. Hasselmann, E. Bauer, P.A.E.M. Janssen, G.J. Komen, L. Bertotti, P. Lionello, A. Guillaume, V.C. Cardone, J.A. Greenwood, M. Reistad, L. Zambresky, and J.A. Ewing, J.A., 1988: The WAM model – a third generation ocean wave prediction model. *J. Phys. Oceanogr.*, 18, 1775–1810

The WISE Group (Cavaleri, L., J.-H.G.M. Alves, F. Ardhuin, A. Babanin, M. Banner, K. Belibassakis, M. Benoit, M. Donelan, J. Groeneweg, T.H.C. Herbers, P. Hwang, P.A.E.M. Janssen, T. Janssen, I.V. Lavrenov, R. Magne, J. Monbaliu, M. Onorato, V. Polnikov, D. Resio, W.E. Rogers, A. Sheremet, J. McKee Smith, H.L. Tolman, G. van Vledder, J. Wolf, and I. Young), 2007: Wave modelling - The state of the art. *Progr. Oceanogr.*, 75, 603-674

Young, I.R., 1999: *Wind generated ocean waves*, Elsevier, 288p.

Young. I.R., M.L. Banner, M.A. Donelan, A.V. Babanin, K.W. Melville, F. Veron, and C. McCormick, 2005: An integrated study of the wind wave source term balance in finite depth water, *J. Atmos. Oceanic Tech.*, 22, 814–828

Zakharov, V.E., and M.M. Zaslavskii, 1983: The shape of the spectrum of the energy containing components of the water surface in the weakly turbulence theory of wind waves. *Izv. Acad. Nauk SSSR, Fiz. Atmos. Okeana,* 10, 1282-1292.

Figure Captions

Figure 1 Comparison of the wave-induced stresses τ'_w (3.4) computed for the wind-source functions of Donelan et al. (2006) (solid line with dots), Donelan (1999) (solid line with asterisks), Hsiao and Shemdin (1983) (solid line with crosses) and Snyder et al. (1981) (solid line with circles), based on JONSWAP spectra in (2-3), - with wave-induced stress τ_w (3.6) (bold line for $C_D(U_{10})$ and bold dashed line for $C_D(U_{10}/c_p)$).

Figure 2 Comparison of wave-induced stresses τ'_w (3.4) computed for the wind-source functions of Donelan et al. (2006) (solid line with dots), Donelan (1999) (solid line with asterisks), Hsiao and Shemdin (1983) (solid line with crosses) and Snyder et al. (1981) (solid line with circles), based on DHH spectra in (2-3), - with wave-induced stress τ_w (3.6) (bold line for $C_D(U_{10})$ and bold dashed line for $C_D(U_{10}/c_p)$).

Figure 3 Comparison of the wind source function of Donelan et al. (2006) before and after applying the coefficient X for the JONSWAP (solid line and line with dots, respectively) and DHH (dashed line and line with crosses, respectively) spectra, with a peak enhancement $\gamma_s = 3.3$, at wind $U_{10} = 10$ m/s.

Figure 4 Smoothing of the results of Figure 3 by means of the stress-correction function $L(f)$ (4-8). Computations were performed for the JONSWAP spectrum.

Figure 5 Comparison of the wind input source function of Donelan et al. (2006) before and after applying the stress-correction function $L(f)$ (4-8). Computations were performed for the JONSWAP (solid line and line with dots, respectively) and DHH (dashed line and line with crosses, respectively) spectra for $U_{10} / c_p = 2.7$ and wind speed $U_{10} = 10$ m/s.

Figure 6 Comparison of growth rate spectra *γ(f)* before and after applying the stress-correction function *L(f)* (4-8). Computations were performed for JONSWAP spectrum for waves with $U_{10} / c_p = 2.7$ and wind speed $U_{10} = 10$ m/s.

Figure 7 Comparison of the growth rate spectra before and after applying the stress-correction function *L(f)* (4-8). Computations were performed for DHH spectrum for waves with $U_{10} / c_p = 2.7$ and wind speed $U_{10} = 10$ m/s.

Figure 8 The wind source function according to Donelan et al. (2006) computed with application of the stress correction function *L(f)* (4-8). Computations were performed for JONSWAP spectra at different stages of wave development with $U_{10} / c_p = 5.8$ (plain lines), 4.5 (line with circles), 2.7 (lines with crosses), 0.83 (lines with dots) for wind speed $U_{10} = 10$ m/s.

Figure 9 The wind source function according to Donelan et al. (2006) computed with application of the stress correction function *L(f)* (Eq. 4-8). Computations were performed for DHH spectra at different stages of wave development with inverse wave age $U_{10} / c_p = 5.8$ (plain lines), 4.5 (line with circles), 2.7 (lines with crosses), 0.83 (lines with dots)} for wind speed $U_{10} = 10$ m/s.

Figure 10 Comparison of the parameter η of the stress correction function *L(f)* (4-9) computed for the wind source function according to Donelan et al. (2006) for

JONSWAP spectra, for $C_D(U_{10})$ (line with dots) and for $C_D(U_{10} / c_p)$ (line with asterisks).

Figure 11 Comparison of the parameter η of the stress correction function $L(f)$ (4-9) computed for the wind source function according to Donelan et al. (2006) for DHH spectra, for $C_D(U_{10})$ (line with dots) and for $C_D(U_{10} / c_p)$ (line with asterisks).

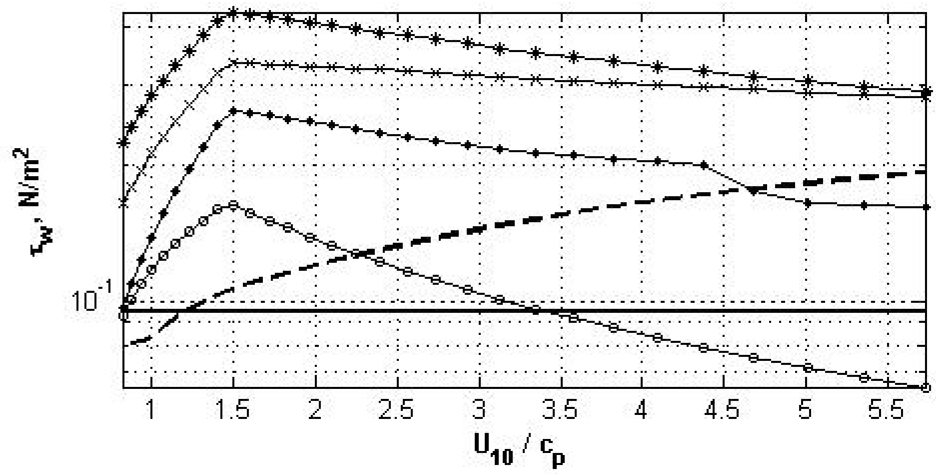

Figure 1 Comparison of the wave-induced stresses τ'_w (3.4) computed for the wind-source functions of Donelan et al. (2006) (solid line with dots), Donelan (1999) (solid line with asterisks), Hsiao and Shemdin (1983) (solid line with crosses) and Snyder et al. (1981) (solid line with circles), based on JONSWAP spectra in (2-3), - with wave-induced stress τ_w (3.6) (bold line for $C_D(U_{10})$ and bold dashed line for $C_D(U_{10}/c_p)$).

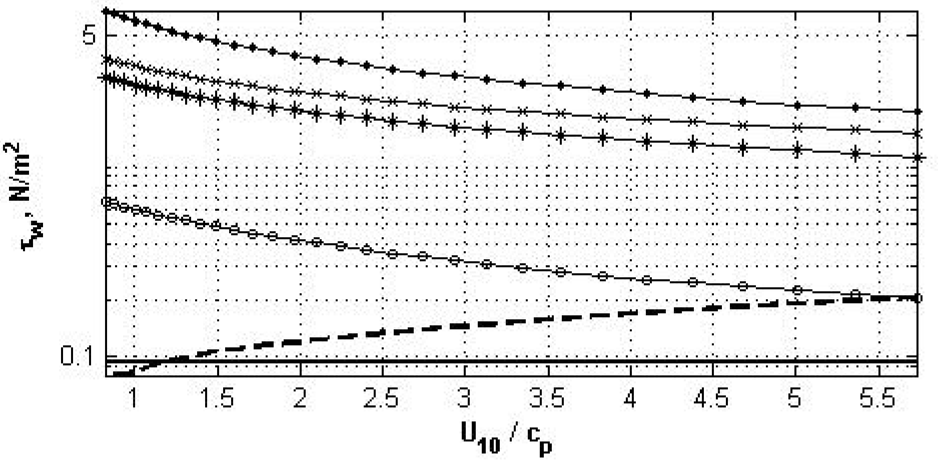

Figure 2 Comparison of wave-induced stresses τ'_w (3.4) computed for the wind-source functions of Donelan et al. (2006) (solid line with dots), Donelan (1999) (solid line with asterisks), Hsiao and Shemdin (1983) (solid line with crosses) and Snyder et al. (1981) (solid line with circles), based on DHH spectra in (2-3), - with wave-induced stress τ_w (3.6) (bold line for $C_D(U_{10})$ and bold dashed line for $C_D(U_{10}/c_p)$).

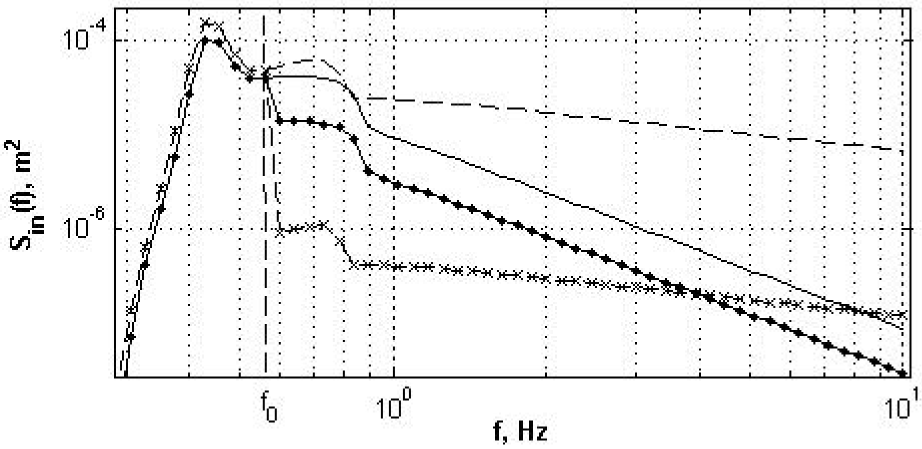

Figure 3 Comparison of the wind source function of Donelan et al. (2006) before and after applying the coefficient X for the JONSWAP (solid line and line with dots, respectively) and DHH (dashed line and line with crosses, respectively) spectra, with a peak enhancement $\gamma_s = 3.3$, at wind $U_{10} = 10$ m/s.

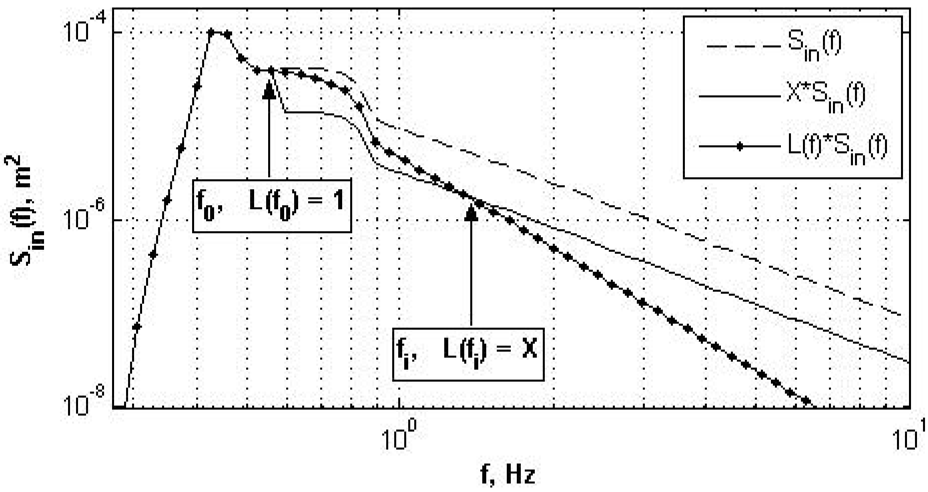

Figure 4 Smoothing of the results of Figure 3 by means of the stress-correction function *L(f)* (4-8). Computations were performed for the JONSWAP spectrum.

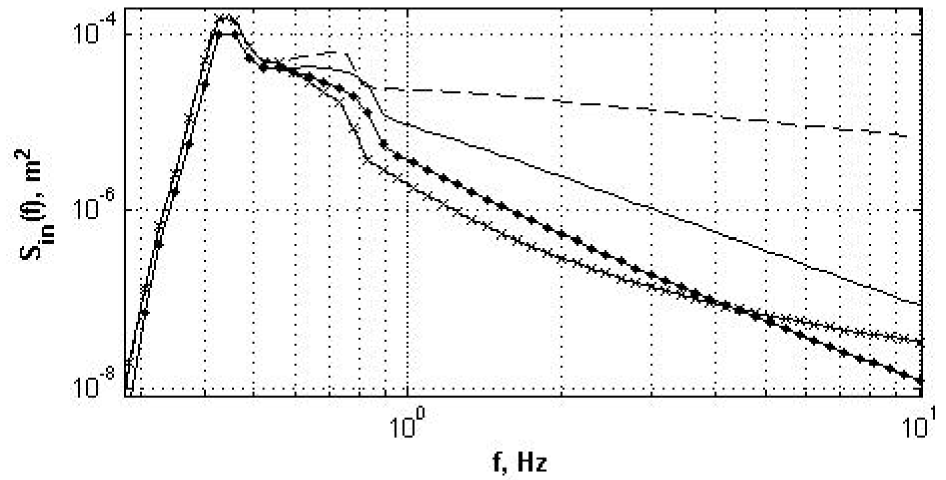

Figure 5 Comparison of the wind source function of Donelan et al. (2006) before and after applying the stress-correction function *L(f)* (4-8). Computations were performed for the JONSWAP (solid line and line with dots, respectively) and DHH (dashed line and line with crosses, respectively) spectra for waves with $U_{10} / c_p = 2.7$ and wind speed $U_{10} = 10$ m/s.

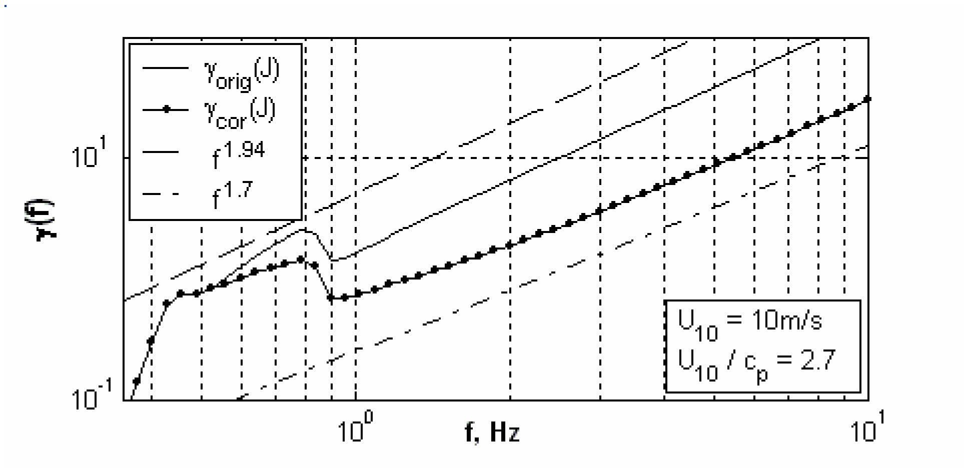

Figure 6 Comparison of growth rate spectra *γ(f)* before and after applying the stress-correction function *L(f)* (4-8). Computations were performed for JONSWAP spectrum for waves with $U_{10} / c_p = 2.7$ and wind speed U_{10} = 10 m/s.

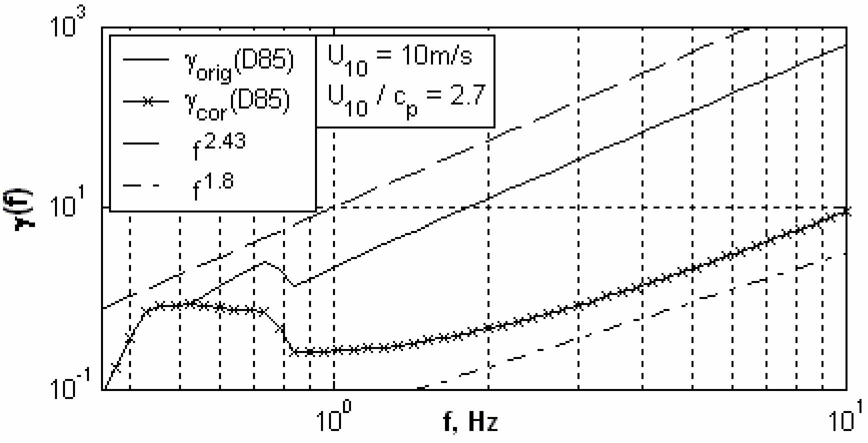

Figure 7 Comparison of the growth rate spectra before and after applying the stress-correction function *L(f)* (4-8). Computations were performed for DHH spectrum for waves with U_{10} / c_p = 2.7 and wind speed U_{10} = 10 m/s.

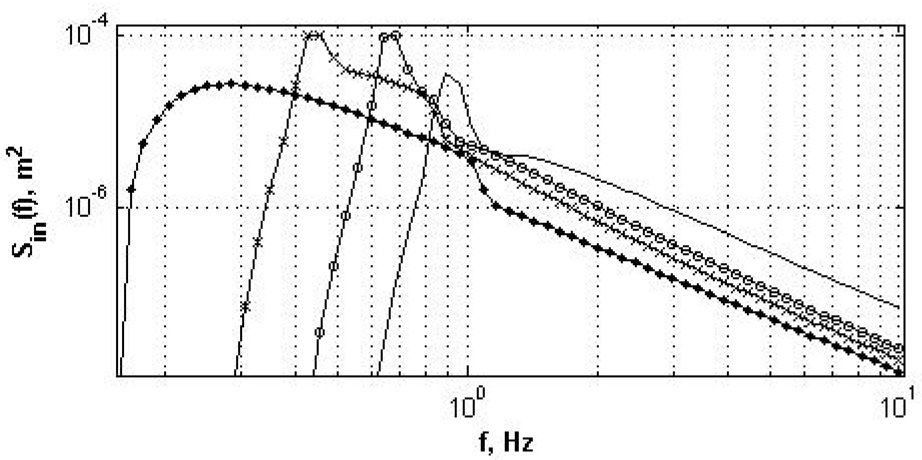

Figure 8 The wind source function according to Donelan et al. (2006) computed with application of the stress correction function *L(f)* (4-8). Computations were performed for JONSWAP spectra at different stages of wave development with U_{10} / c_p = 5.8 (plain lines), 4.5 (line with circles), 2.7 (lines with crosses), 0.83 (lines with dots) for wind speed U_{10} = 10 m/s.

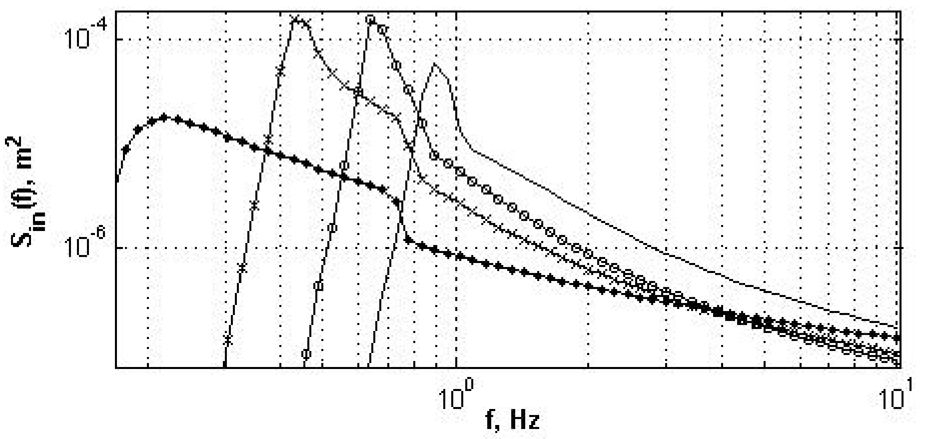

Figure 9 The wind source function according to Donelan et al. (2006) computed with application of the stress correction function *L(f)* (Eq. 4-8). Computations were performed for DHH spectra at different stages of wave development with inverse wave age U_{10} / c_p = 5.8 (plain lines), 4.5 (line with circles), 2.7 (lines with crosses), 0.83 (lines with dots)} for wind speed U_{10} = 10 m/s.

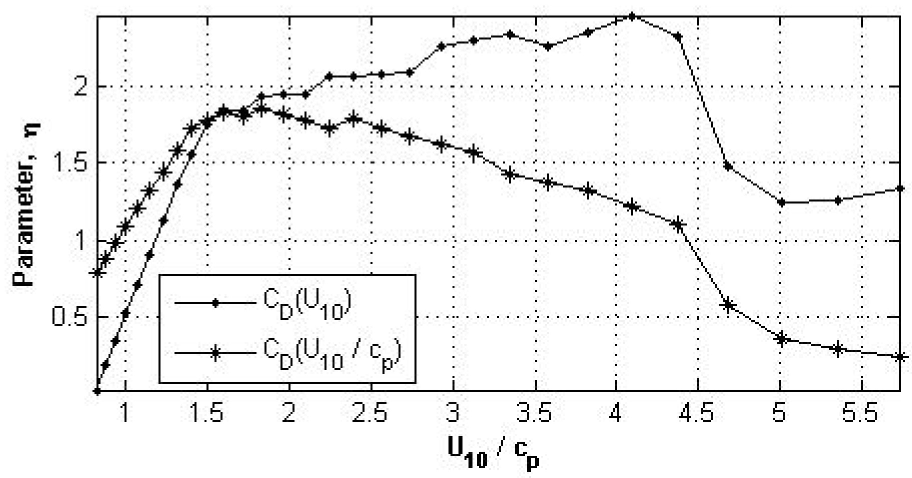

Figure 10 Comparison of the parameter η of the stress correction function *L(f)* (4-9) computed for the wind source function according to Donelan et al. (2006) for JONSWAP spectra, for $C_D(U_{10})$ (line with dots) and for $C_D(U_{10} / c_p)$ (line with asterisks).

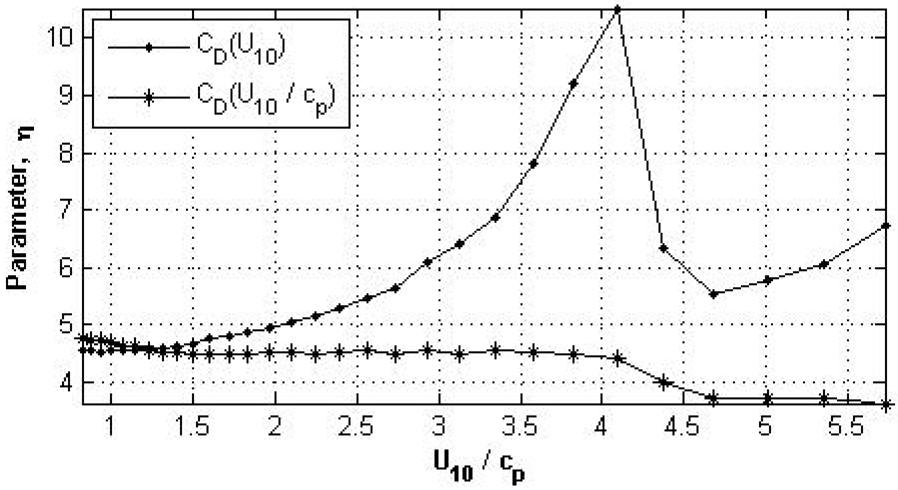

Figure 11 Comparison of the parameter η of the stress correction function *L(f)* (4-9) computed for the wind source function according to Donelan et al. (2006) for DHH spectra, for $C_D(U_{10})$ (line with dots) and for $C_D(U_{10}/c_p)$ (line with asterisks).